Tellus SERIES B CHEMICAL AND PHYSICAL METEOROLOGY
PUBLISHED BY THE INTERNATIONAL METEOROLOGICAL INSTITUTE IN STOCKHOLM

Towards the improvements of simulating the chemical and optical properties of Chinese aerosols using an online coupled model – CUACE/Aero

By CHUN-HONG ZHOU[1,2]*, SUNLING GONG[1,3], XIAO-YE ZHANG[1], HONG-LI LIU[1], MIN XUE[1], GUO-LIANG CAO[4], XING-QIN AN[1], HUI-ZHENG CHE[1], YANG-MEI ZHANG[1] and TAO NIU[1], *[1]Key Laboratory for Atmospheric Chemistry, Chinese Academy of Meteorological Sciences, Beijing 100081, China; [2]Graduate University of Chinese Academy of Science, 19A Yuquanlu Shijingshan District, Beijing 100049, China; [3]Air Quality Research Division, Science & Technology Branch, Environment Canada, 4905 Dufferin Street, Toronto ON M3H 5T4, Canada; [4]School of Environmental and Municipal Engineering, Xi'an University of Architecture and Technology, Xi'an 710055, China*

(Manuscript received 18 October 2011; in final form 31 May 2012)

ABSTRACT

CUACE/Aero, the China Meteorological Administration (CMA) Unified Atmospheric Chemistry Environment for aerosols, is a comprehensive numerical aerosol module incorporating emissions, gaseous chemistry and size-segregated multi-component aerosol algorithm. On-line coupled into a meso-scale weather forecast model (MM5), its performance and improvements for aerosol chemical and optical simulations have been evaluated using the observations data of aerosols/gases from the intensive observations and from the CMA Atmosphere Watch network, plus aerosol optical depth (AOD) data from CMA Aerosol Remote Sensing network (CARSNET) and from Moderate Resolution Imaging Spectroradiometer (MODIS). Targeting Beijing and North China region from July 13 to 31, 2008, when a heavy hazy weather system occurred, the model captured the general variations of PM10 with most of the data within a factor of 2 from the observations and a combined correlation coefficient (r) of 0.38 (significance level = 0.05). The correlation coefficients are better at rural than at urban sites, and better at daytime than at nighttime. Chemically, the correlation coefficients between the daily-averaged modelled and observed concentrations range from 0.34 for black carbon (BC) to 0.09 for nitrates with sulphate, ammonium and organic carbon (OC) in between. Like the PM10, the values of chemical species are higher for the daytime than those for the nighttime. On average, the sulphate, ammonium, nitrate and OC are underestimated by about 60, 70, 96.0 and 10.8%, respectively. Black carbon is overestimated by about 120%. A new size distribution for the primary particle emissions was constructed for most of the anthropogenic aerosols such as BC, OC, sulphate, nitrate and ammonium from the observed size distribution of atmospheric aerosols in Beijing. This not only improves the correlation between the modelled and observed AOD, but also reduces the overestimation of AOD simulated by the original model size distributions of primary aerosols. The normalised mean error has been reduced to 62% with the CARSNET observations and 76% with MODIS, from the original 111% and 143%, respectively. The factors resulting in the underestimation of aerosol concentrations and other discrepancies in the model are explored, and improvements in enhancing the model performance are proposed from the analysis. It is found that the accuracy in meteorological predictions plays a critical role on the simulation of the occurrence and accumulation of heavy pollution episode, especially the circulation winds and the treatment of Planetary Boundary Layer (PBL).

Keywords: CUACE/Aero, on-line coupled model, aerosol, AOD

1. Introduction

Atmospheric aerosols not only deteriorate the natural environment, but also harm human health and have direct and indirect impacts on weather and climate (Twomey,

*Corresponding author.
email: zhouch@cma.gov.cn

Citation: Tellus B 2012, **64**, 18965, http://dx.doi.org/10.3402/tellusb.v64i0.18965

1991; Jones et al., 1994; Charlson and Heintzenberg, 1995; Yu, 2000; Ramanathan et al., 2001; Yu et al., 2001; Caminade et al., 2006; IPCC, 2007). In many regions around the globe, aerosols are the major pollutants in the atmosphere, and their fine fractions are also the main factors leading to the poor visibility (Mam et al., 2004). The question as how to address these impacts of aerosols has always been a focus of attention and a challenge for the scientific community (Adams et al., 2000; Bertrand et al., 2002; Brook et al., 2002; Fast et al., 2005; Levin and Cotton, 2009). In addition, atmospheric aerosols are composed of a variety of components, which vary in size with different sources. They are subject not only to atmospheric thermodynamics and aerosol microphysics and dynamics, but also to mutual interactions, which make it a challenge to simulate them properly (Jacobson et al., 1997; Zhang et al., 1999).

Surface-based observations, satellite retrieval and direct emission inventories have shown the growing impairment of air quality (AQ) in East Asia in the last 30 yr (Streets et al., 2003; Richter et al., 2005; Cao et al., 2006; Zhang et al., 2011). Particulate matters (PM), i.e. aerosols, are the major pollutants in the atmosphere with the annual mass concentration of 100 $\mu g\ m^{-3}$ over China (Qu et al., 2010), much higher than those in North America or Europe. Sources for these particles and their precursors consist of large amounts of carbonaceous matters, fugitive dust, NO_X, SO_2, CO, NH_3 and C_xH_y from industry, agriculture, transportation, civil life and natural mineral dust from dry areas of northwest China, deserts of Mongolia. A number of models have been developed and used to simulate the PM other than mineral dust aerosol in East Asia in several projects, e.g. TRACER-P, ACE-Asia and MICS-ASIA projects (Chin et al., 2003; Gong et al., 2003b; Zhang et al., 2003; Tang et al., 2004; Tsai et al., 2004; Carmichael et al., 2008) and the Cloud Indirect Forcing Experiment (CIFEX) (Wilcox et al., 2006) and the East Asian regional Experiment (EAREX) (Nakajima et al., 2007). However, due to different purposes, those works were mostly focused on aerosols in the outflow of Asian continent or in Asian mega cities. None of these models were developed to deliver operational aerosol or AQ forecasts over the whole China. More works are needed on the simulation and detailed evaluation of the aerosol distribution and its optical characteristics over the main continent over China in order to provide more accurate forecasts for PM and visibility.

CUACE/Aero, China Meteorological Administration (CMA) Unified Atmospheric Chemistry Environment/Aerosol, a fully online coupled meteorological/chemistry/aerosol system, has been developed for aerosol simulation and for the investigation of its impacts on AQ forecasts in Asia where high concentrations and complex chemical compositions of aerosols exist. This paper is to explore the factors influencing the accuracy of the model simulations through a detailed evaluation of model performance with observation data and sensitivity tests targeting Beijing and North China. Consequently, the research is to provide an insight into the controlling components to achieve more accurate aerosol simulations in China and hence to enhance the AQ forecasts, which have not been fully investigated before. Specifically, the impacts of initial size distributions of primary PM emissions on the simulation of optical properties [e.g. aerosol optical depth (AOD)] in China were examined to search for more accurate parameters to reduce the uncertainties of AQ forecasts related to the degradation of visibility by the increase of aerosols.

In the following, the model description, sensitivity experiment setups and data sets are presented in Section 2, followed by the analysis of the results in Section 3, and discussion and summary are presented finally in Section 4.

2. Description of model and experiments

2.1. CUACE/Aero

CUACE is a unified atmospheric chemistry environment with four major functional sub-systems, emissions, gas phase chemistry, aerosols and data assimilation, and is developed to facilitate the establishment of a chemical weather forecasting system using near real-time data in China. One of its sub-systems, CUACE/Aero, is a comprehensive module incorporating emission, gaseous chemistry and size-segregated multi-component aerosol algorithms. Using the national official basic information of emission sources published in 2005 and updated with 83 point-sources for anthropogenic emissions over China at a resolution of $0.5^\circ \times 0.5^\circ$ (Cao et al., 2005, 2006; Lang et al., 2008), the Emission Subsystem (EMIS) provides, through SMOKE (The Sparse Matrix Operator Kernel Emissions) module, the hourly gridded off-line emission intensity for 32 species including black carbon (BC), organic carbon (OC), sulphate, nitrate, fugitive dust particles and 19 volatile organic compounds (VOC), NH_3, CO, CO_2, SO_x and NO_x over the model domain. The gas chemistry module is based on the second generation of Regional Acid Deposition Model (RADM II) mechanism with 63 gaseous species through 21 photo-chemical reactions and 121 gas phase reactions applicable under a wide variety of environmental conditions especially for smog (Stockwell et al., 1990). There are seven categories of aerosol species, i.e. sea salts, sand/dust, BC, OC, sulphates, nitrates and ammonium salts in the aerosol module. Natural sea salt emission is calculated on-line with the parameterisation scheme developed by Gong (2003) which improves the sea salt simulation for number density and size distribution under 0.1 μm. The natural sand/dust

emissions are simulated with the Marticorena–Bergametti–Alfaro (Marticorena and Bergametti, 1995; Alfaro and Gomes, 2001) scheme by carefully using data representing the desert layouts, soil textures and dust aerosol size distributions over China (Gong et al., 2003b; Zhao et al., 2003; Zhou et al., 2008). Apart from natural emissions, fugitive dust from construction and transportation has also been taken into account as the dust emission.

The aerosol microphysics contains major aerosol processes in the atmosphere such as hygroscopic growth, coagulation, nucleation, condensation, dry depositions, scavenging and aerosol activations (Gong et al., 2003a), which is coherently integrated with the gaseous chemistry in CUACE/Aero. The gaseous chemistry provides the production rates of sulphate and second organic aerosols (SOA), and at the same time generates an oxidation background for aqueous phase aerosol chemistry, in which sulphate transformation changes the distributions of SO_2 in clouds. Both nucleation and condensation are considered for sulphate aerosol formation depending on the atmospheric state after gaseous H_2SO_4 formed from the oxidation of sulphurous gases such as SO_2, H_2S and DMS. Second organic aerosols as generated from gaseous precursors are partitioning among different bins through condensation using the same approach as the gaseous H_2SO_4 condensation to sulphate. Since the nitrates and ammonium formed through the gaseous oxidation are unstable and prone to further decomposition back to their precursors, CUACE adopts ISSOROPIA to calculate the thermodynamic equilibrium between them and their gas precursors (West et al., 1998; Nenes et al., 1998, Yu et al., 2005). Table 1 shows the list of the specific parameterisation schemes for various CUACE components. Except for ammonium, sulphates, BC, OC, sand/dust, nitrates and sea salts are segregated into 12 size bins with radii ranging from 0.005–0.01, 0.01–0.02, 0.02–0.04, 0.04–0.08, 0.08–0.16, 0.16–0.32, 0.32–0.64, 0.64–1.28, 1.28–2.56, 2.56–5.12, 5.12–10.24, 10.24–20.48 μm. In each size bin, an internal mixture is assumed for all aerosol components, while external mix is adopted between different bins for the particle number density.

In this study the CUACE/Aero is on-line coupled into MM5 to achieve synchronous integrations and outputs of various species and meteorological elements. Its horizontal dimensions are set to 136×169 at a resolution of 54 km to cover Asia and the eastern part of Europe. There are 24 vertical sigma levels up to 100 hPa with the level thickness increasing with height. In the coupled system, the large-scale transports of various tracers are based on the positive and conserved advection transport algorithm scheme (MPDATA) (Smolarkiewicz, 2006) and the diffusivity from the nonlocal diffusion originally for heat and humidity in MRF PBL scheme which has been used in CUACE/Dust (Zhou et al., 2008).

2.2. *Experimental scheme and observation database*

Three sets of experimental runs were designed: the control run (CTL), sensitive test one (ST1) and test two (ST2). For all the runs, the evaluation period was selected from July 13 to 31, 2008, during which a very heavy hazy episode persisted from July 22 to 28 in North China. The initial and boundary values for O_3 and OH radical were taken from climatic means, and zeros for each aerosol species at July 4 with a 10-day spin-off run to achieve full mixing for gas chemistry and aerosols. The initial and boundary meteorological fields are interpolated from the 6-hour analysis of CMA T213 model, including wind, temperature, pressure and humidity at each standard level from the ground to 100 hPa for the CTL run. In order to explore the impacts of meteorological fields on the under-estimates of PM10 during the heavy hazy episode, the experimental ST1 run from July 22 to July 28 was done by replacing the meteorology of July 22–25 with that of July 25–28, which was more close to the reality than the originally provided by T213 model. In the experimental ST2 run, a new set of initial mass and number size distributions for BC, OC, SF, nitrate and fugitive dust were used to investigate the impacts of initial size distributions on the AOD simulations.

The targeting area for the evaluation is defined by 110° E–120°E, 34°N–42°N covering North China (Fig. 1). Three kinds of observations are used for the model evaluation. First, the mandatory meteorological observations of wind, temperature, pressure and humidity are available from eight stations in the region where *Zhangjiakou*, *Nanjiao*, *Jinan*,

Table 1. CUACE components and algorithms

Gas phase chemistry	RADM II [Stockwell et al., 1990]
SOA formation	Gas/particle partitioning (Schell et al., 2001)
Aqueous-phase chemistry	Gery et al. (1989)
Aerosol physics	CAM (Gong, 2003)
Inorganic heterogeneous chemistry	ISORROPIA (Nenes et al., 1998)
Vertical diffusion	K-theory eddy diffusivity from MRF scheme (Zhou et al., 2008)
Advection	MPDATA (Smolarkiewicz, 2006)

SOA, second organic aerosols.

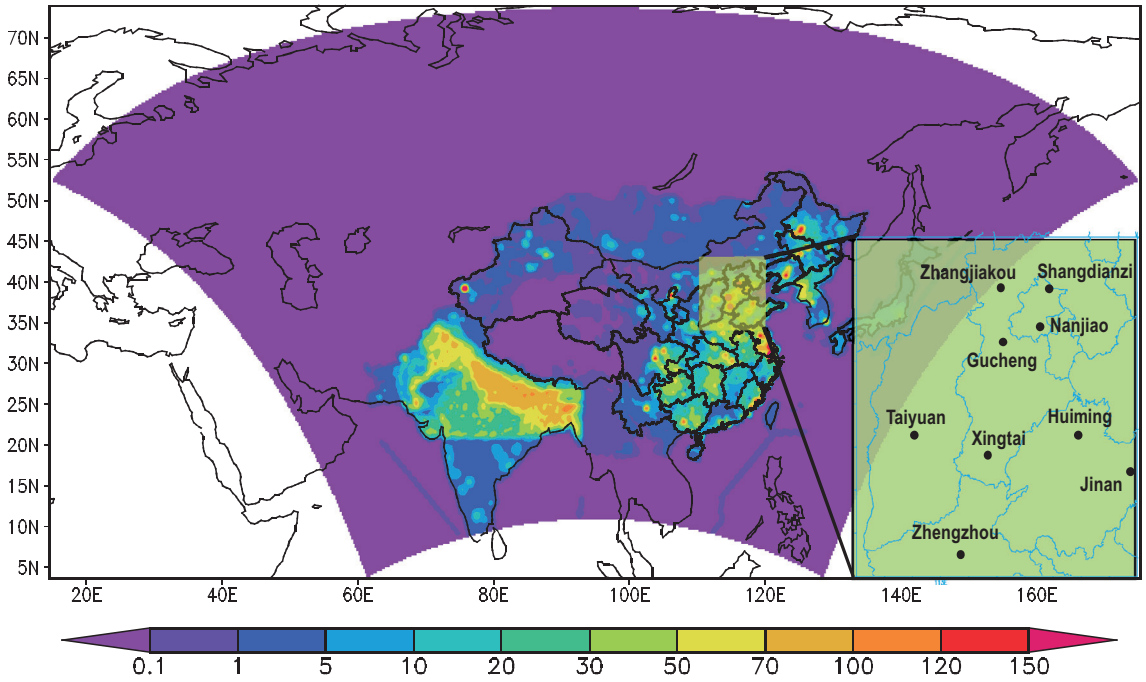

Fig. 1. The model domain, results domain and stations. The background is BC emission at the unit of kg gird^{-1} s^{-1}.

Xingtai, *Zhengzhou* and *Taiyuan* have both upper air (twice daily) and surface (eight times daily) observations, with *Shangdianzi* and *Huimin* having only surface observations. Second, the surface daily and hourly PM10 and BC concentrations from CMA Atmosphere Watch network (CAWNET) and AOD data from CMA Aerosol Remote Sensing network (CARSNET) are obtained at five stations (hereinafter referred to as the five stations) (Zhang et al., 2008): *Shangdianzi*, *Nanjiao*, *Gucheng*, *Zhengzhou* and *Huimin* (Table 2). AOD from NASA Moderate Resolution Imaging Spectroradiometer (MODIS) has also been used for its large spatial coverage. Finally, SO_2, aerosol number concentrations and the water-soluble aerosol data with diameter less than 1 μm were obtained at the intensive observation campaign at a CMA site (Zhang et al., 2009). All the model outputs have been interpolated through the Cressman Scheme with a radius of 0.5° into the observation stations (Cressman, 1959). The MODIS AODs have been interpolated into the model grids with a radius of 0.3°. In addition to the scatter and time series plots, model statistics are presented in Table 3 for the mean bias (MB), normalised mean bias (NMB), mean errors (ME), normalised mean errors (NME) and correlation coefficient (*r*) (Yu et al., 2006, 2008).

Table 2. Name, type and observation elements for the five CAWNET/CARSNET Stations

Shangdianzi	Regional background	PM10, AOD
Nanjiao	Urban	PM10, AOD
Gucheng	Rural	PM10, AOD
Huimin	Rural	PM10, AOD
Zhengzhou	Urban	PM10, AOD

3. Analysis of experimental results

3.1. *Evaluation of the meteorological fields of MM5-CUACE/Aero*

Meteorological performance is critical in achieving a good prediction of chemical species in the atmosphere. It is directly linked to the transport, diffusion, chemistry, hygroscopic growth, deposition and interactions of aerosols and their precursors. Gridded model outputs of wind speed/direction, temperature, humidity and geopotential height at ground, 850, 700 and 500 hPa have been interpolated in the eight meteorological stations and compared with surface and upper layer radiosondes data (Table 4).

The analysis shows that the temperature correlation coefficients at three upper levels are all larger than 0.85 with the mean square errors (MSE) of less than 1.6 K except for 850 hPa with a correlation coefficient of 0.77. The wind speed simulation is more complicated than the temperature and height fields. However, the wind speed correlation at 850 hPa level reaches 0.6 and gets better with heights. Mean square errors at all levels are very small, basically around 2.5 m s^{-1}, except for 500 hPa. The correlations for wind direction are better than those for the wind speed at all levels. Mean square errors of wind

Table 3. Statistical metrics used for performance evaluation

Mean bias (MB); mean difference (MD)	$(1/n)\sum_i (m_i - o_i)$
normalised mean bias (NMB); normalised mean difference (NMD)	$\left[\sum_i (m_i - o_i)/\sum_i o_i\right] \times 100\%$
Mean error (ME); mean absolute difference (MAD)	$(1/n)\sum_i \lvert m_i - o_i\rvert$
Normalised mean error (NME); normalised mean absolute difference (NMAD)	$\left[\sum_i \lvert m_i - o_i\rvert/\sum_i o_i\right] \times 100\%$
Coefficient of determination (r^2)	$r^2 = 1 - \mathrm{SSE/SST}$; $\mathrm{SSE} = \sum_i (m_i - m_i')^2$; $\mathrm{SST} = \sum_i m_i^2 - (1/n)\cdot\left(\sum_i m_i\right)^2$; $m_i' = a + b \cdot o_i$

Note: n is the total number of data pairs and $i = 1, 2, \ldots, n$, o is the measured concentration and m is the modelled concentration.

direction at all level are less than 20° at upper levels. Because pollutants are mainly concentrated in the mid and lower troposphere, the error of the simulated wind speed in the lower troposphere should affect their transport and diffusion. The analysis of humidity suggests that the correlation from 850 to 500 hPa is similar, i.e. >0.50. The MSE for humidity is also small at lower levels and increases slightly with height, which indicates that the outcome of the simulated humidity at mid and lower levels is better than that at higher levels. This may be conductive to some processes such as deposition and transformation related to aerosol and humidity. For the surface layer, the correlation coefficients for all the other variables can reach 0.6 with small deviation compared to the higher levels except the wind speed whose correlation coefficient is only 0.26, which has an adverse impact on the model performance as discussed later.

Compared to the evaluation of the meteorological fields simulated by MM5 in summer time [Dilley et al., 2003] in the USA, the current system has the equivalent performance with small and reasonable atmosphere standard deviations and correlations.

3.2. Comparison of CUACE PM10 with observations

The statistical results and scatter plots for all the simulated and the observed daily averaged PM10 for the five stations in CTL run are summarised as shown in Table 5 and in Figure 2. It can be seen that the model captured the general variations of PM10 with most of the data having a factor of 2 within the observations and a combined correlation coefficient (r) of 0.38 (Fig. 2). The mean observed PM10 for *Shangdianzi* is the lowest among the five stations due to the fact that *Shangdianzi* is dedicated as the regional pollution background site for North China Plain in CAWNET with aged particles from south and little local emissions. However, for the rural sites of *Huimin* and *Gucheng,* the mean PM10 concentrations have reached 101.3 and 95.5 μg m^{-3} respectively, which are comparable to the high values for the urban sites of *Beijing Nanjiao* and *Zhengzhou*. This indicates that compared to urban areas, particulate pollution in the rural areas is also very high. The NMB in *Huimin* is -31.1% with an NME of 43.5%, indicating that there is an obvious systematic underestimation of PM10 in this site. The NMBs in rural sites of *Shangdianzi* and *Gucheng* are near to or lower than 10%, much less than for other three stations. For the rural sites *Huimin* and *Shangdianzi*, the correlation coefficients are 0.52 and 0.40, respectively, being on the top among the five stations.

In Table 5, the correlation coefficients at daytime for the five stations are all higher than those at nighttime while the aerosol concentrations at daytime are all underestimated, as the MBs and NMBs are all negative and NMBs are comparable to NMEs. By a careful examination of the

Table 4. Comparison between observations and simulations of meteorological fields

Meteorological field	Quantity	Ground	850 hPa	700 hPa	500 hPa
Temperature	r	0.61	0.77	0.93	0.89
	MSE (K)	3.3	1.6	1.1	1.8
Humidity	r	0.55	0.51	0.67	0.54
	MSE (%)	13.2	14.0	21.3	21.2
Wind speed	r	0.26	0.64	0.64	0.82
	MSE (ms^{-1})	0.55	2.5	2.5	4.1
Wind direction	r	0.54	0.92	0.90	0.90
	MSE (°)	28	15	13	10

Note: r is the correlation coefficient (significance level = 0.0500), and at ground use pressure for the element of geo-potential height. MSE, mean square error.

Table 5. Simulated mean (model mean) and mean observed (observed mean) PM10 concentrations, and mean bias (MB), NMB (normalised mean bias), NME (normalised mean errors and correlation coefficient *r* for nighttime, daytime and full day (daily) of the five stations: Shangdianzi, Nanjiao, Gucheng, Huimin and Zhengzhou for CTL test

Stations	Model mean	Observed mean	MB	NMB (%)	NME (%)	*r*
Shangdianzi						
Daytime	37.9	56.4	−18.5	−32.8	46.0	0.61
Nighttime	64.4	61.5	2.8	4.6	71.5	0.15
Daily	51.1	59.3	−8.2	−13.7	56.7	0.40
Nanjiao						
Daytime	65.2	116.6	−51.4	−44.1	44.1	0.27
Nighttime	135.9	138.4	−2.5	−1.7	47.6	−0.08
Daily	100.5	127.7	−27.2	−21.3	37.4	−0.01
Gucheng						
Daytime	69.7	100.2	−30.4	−30.4	38.8	0.39
Nighttime	121.3	102.7	18.6	18.1	46.6	0.13
Daily	95.5	101.3	−5.8	−5.7	35.1	0.20
Huimin						
Daytime	50.4	93.3	−42.9	−46.0	53.3	0.54
Nighttime	81.0	96.9	−15.8	−16.2	54.3	0.33
Daily	65.8	95.5	−29.7	−31.1	43.5	0.52
Zhengzhou						
Daytime	58.7	96.0	−37.3	−38.9	44.0	−0.19
Nighttime	120.7	96.7	24.0	24.8	68.9	0.18
Daily	89.7	96.6	−6.9	−7.1	38.6	0.05

Significance level = 0.0500.

PBL simulations from the model, it was found that the performance was closely linked to the simulation of PBL heights. The modelled mixing heights varied from 1500 to 3000 m high at daytime and were only about 40 m (the height of the first layer of the model) at night for both rural and urban sites (Fig. 3). While the observed mixing layer heights are typically around 1000 m high in clear days and would be much lower under stable weather conditions in summer (He et al., 2006). This implied that aerosols in the near surface had been over-diluted in the daytime due to the over-estimate of the PBL heights. It has been found that the MRF PBL scheme used in this MM5 tends to produce over-developed PBL in the daytime even at very high horizontal resolutions (about 2 km) (Hong and Noh, 2006; Steeneveld et al., 2008).

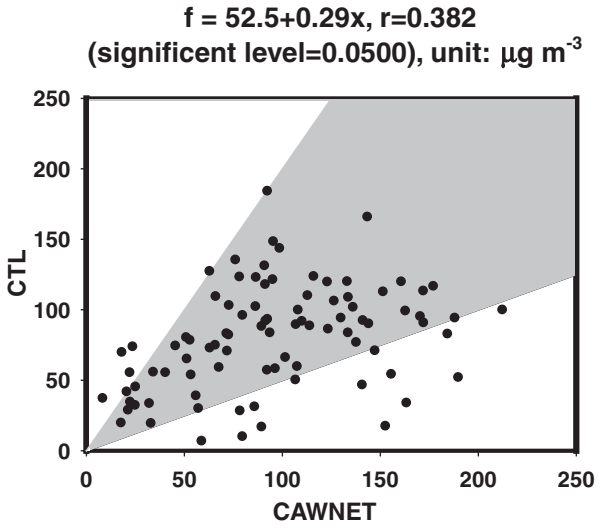

Fig. 2. Scatters of simulated and observed daily mean PM10 for all the five stations in CTL run. Results of CTL means from control run. CAWNET is from CAWNET observation.

On the contrary, at night, there are no underestimations, and the MBs and NMBs for all stations are much less than those for the daytime. However, the NMEs are much larger than the NMBs and are all much larger than those of the daytime, which indicates that there exit larger random errors in the simulation at night than at the daytime. These random errors are found to be related to the MRF PBL scheme which roughly defines the PBL regime to be stable when the Bulk Richardson Number is larger than 0.5 and cannot represent the significant turbulence generated mainly by short-term (minutes) accelerations of unknown origin in the near-calm nocturne conditions (Mahrt et al., 2012).

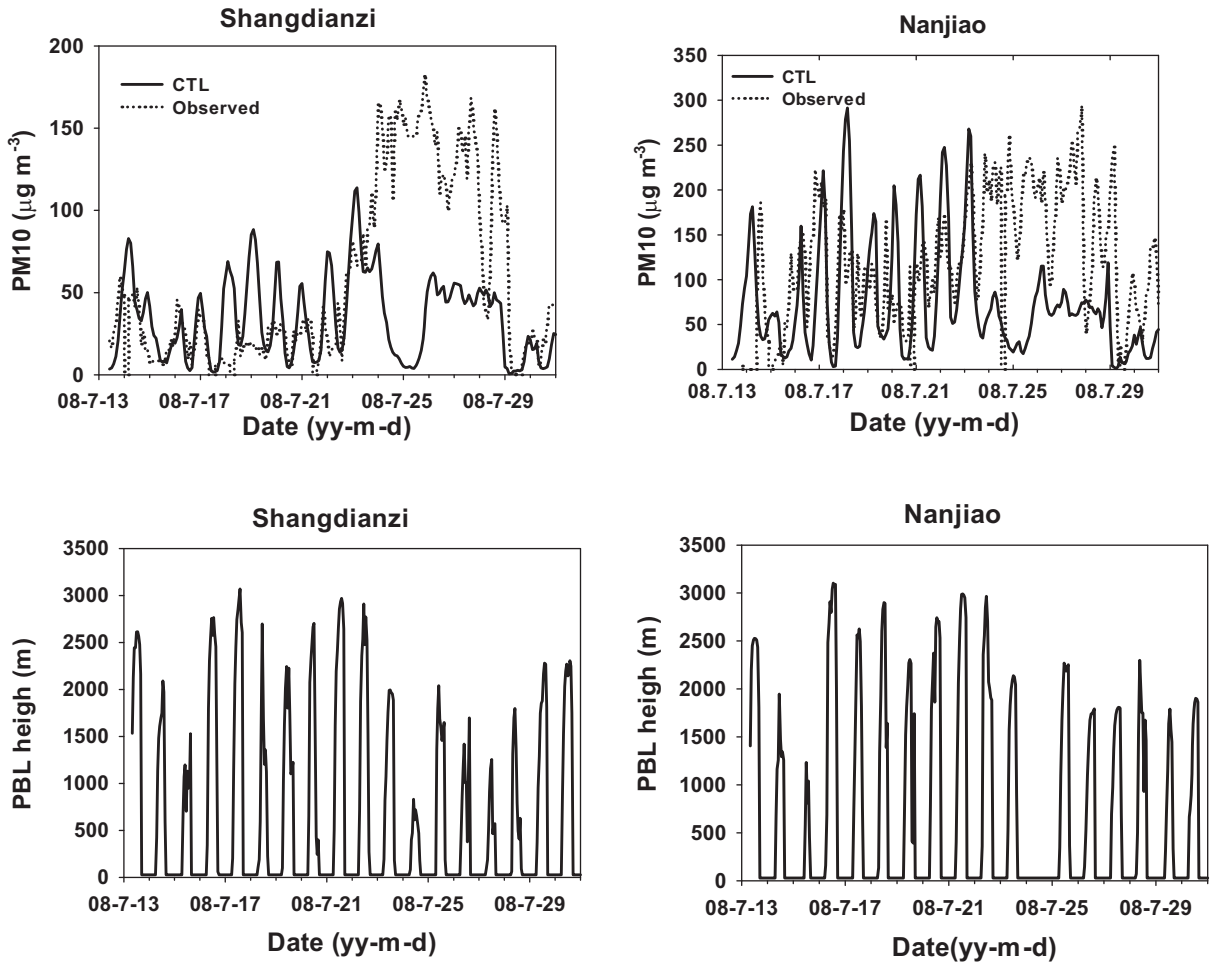

Fig. 3. Upper panel: time series of simulated and observed hourly PM10 in two-hour interval for typical rural site: Shangdianzi (left) and urban site: Nanjiao (right) in CTL. Results of CTL means from the control run. Observed is the observation. Bottom panel: time series of hourly PBL heights for Shangdianzi (left) and Nanjiao (right).

Of cause, the model resolution is also a factor contributing to the poor simulation of PBL height. The coarse resolution and the missing updated database to represent the rapid growth of the urban areas and changes of the landuse and landcover in North China have definitely contributed to the unrealistic simulation of PBL in the model and needs to be improved in future studies.

3.3. Comparison of aerosol constituents in Beijing

One aerosol mass spectrometer (AMS) and one 43CTL SO_2 analyser (Thermal Environmental, USA) stationed on a CMA building in the centre of Beijing City measured the diurnal variation of the sub-micron hydroscopic aerosol constituents and SO_2 from June 20, 2008. One Aethalometer (model AE-31, Magee Scientific) was used to measure BC on a 5-min time base at *Nanjiao* (Zhang et al., 2009). The daily, day- and nighttime mean aerosol concentrations of OC, sulphate, nitrate, ammonium and BC from both observations and CTL simulations are shown in Table 6.

The correlation coefficients between daily-averaged modelled and observed concentrations range from 0.34 for BC to 0.09 for nitrates with sulphate, ammonium and OC in between. Generally, the correlation values are higher for the daytime than those for the nighttime, which is very similar to the PM10, and underestimations are shown for all the hygroscopic aerosol components. The OC concentrations are very close to observations with an NMB of about −10% and NME of 24%. The sulphate, ammonium and nitrate are underestimated by about 59.7, 70 and 96.0%, respectively. It is showed that SO_2 is overestimated by 54% in Beijing (Table 6). However, an analysis of the OH radicals in the model points out to the underestimated oxidation capacity of the atmosphere in North China. Observations show that the concentration of OH radical

Table 6. Simulated mean (model mean) and mean observed (observed mean) concentrations, MB (mean bias), NMB (normalised mean bias), NME (normalised mean errors and correlation coefficient r for nighttime, daytime and full day (daily) of the five aerosol constituents: sulphate (SF), organic carbon (OC), ammonia (AM), nitrate (NT) and BC in control run (CTL)

Aerosol constituents	Model mean	Observed mean	MB	NMB (%)	NME (%)	r
SF						
Daily	13.4	33.2	−19.8	−59.7	60.7	0.284
Daytime	11.3	32.1	−20.8	−64.9	64.9	0.57
Nighttime	15.5	34.3	−18.8	−54.8	59.8	−0.12
OC						
Daily	27.2	30.5	−3.3	−10.8	24.4	0.124
Daytime	17.0	29.3	−12.3	−42.0	42.5	0.33
Nighttime	37.3	31.3	6.0	19.0	34.5	0.31
NH_4^-						
Daily	4.5	14.9	−10.4	−70.1	70.1	0.284
Daytime	3.1	13.8	−10.7	−77.6	77.6	0.68
Nighttime	5.8	16.0	−10.1	−63.4	63.9	−0.04
NO_3^-						
Daily	0.6	15.9	−15.3	−96.0	96.0	0.09
Daytime	0.2	12.7	−12.5	−98.8	98.8	0.22
Nighttime	1.1	18.8	−17.7	−94.0	94.0	0.15
BC						
Daytime	7.8	4.4	3.4	80.1	80.1	0.47
Nighttime	17.5	6.7	10.8	161.0	165.3	0.42
Daily	12.7	5.5	7.1	129.0	129.2	0.34
SO_2						
Daytime	8.9	5.5	3.4	38.0	52.2	0.33
Nighttime	15.2	5.4	9.8	64.0	70.0	0.14
Daily	11.8	5.4	6.3	54.0	62.9	0.19

Significance level = 0.0500.

can reach 8×10^7 cm^{-3} in summer time in Beijing (Ren et al., 2002) and about 10^6 cm^{-3} in the outflow atmosphere of the Asia in west Pacific Ocean (Crawford et al., 2003). However, the highest values of OH radicals from the gas chemistry in the model are only close to 10^5 cm^{-3} (1 ppt) which is around the global background value and is about two to three orders of magnitude lower than the observed value in Beijing. The lower oxidation capacity was a factor for the underestimation of sulphate and nitrate since most days were clear during the test time with clear sky processes dominated. The ammonium has also been underestimated by 70% and has a ratio of 1:3 to the sulphate mass concentrations from the model, indicating that almost all the ammonia was combined with sulphuric acid to form the ammonium sulphate with very little left for nitric acid. The observed ammonium to sulphate ratio is close to 1:2, which shows that abundant ammonia can be combined with nitrate acid in reality. Urban areas are rich in ammonia because of emissions, i.e. from coal combustions (Cao et al., 2010) which have not been fully accounted for in the emission database for ammonia in the current modelling system. The underestimation of ammonium is also a major reason for the underestimation of nitrate. Therefore, a reasonable simulation of ammonium is the basis for improving the sulphate and nitrate simulations.

Only BC was overestimated by 129%, with 80% higher at daytime and 165% higher at night, respectively. However, due to the small fraction of BC in the total aerosol, e.g. 3% in 127.7 μg m^{-3} PM10 at *Nanjiao*, the overestimation of BC did not change the general underestimation trend of total PM10 in the region.

3.4. Aerosol under a heavy hazy episode

A heavy PM episode was observed from July 22 to 28, during which time North China was controlled by a combination of a strong subtropical high and a continental high and a stable weather featuring light fog with haze observed (Fig. 4a). The weather map at 500 hPa at 00 UTC on July 26 indicated that North China was just under the

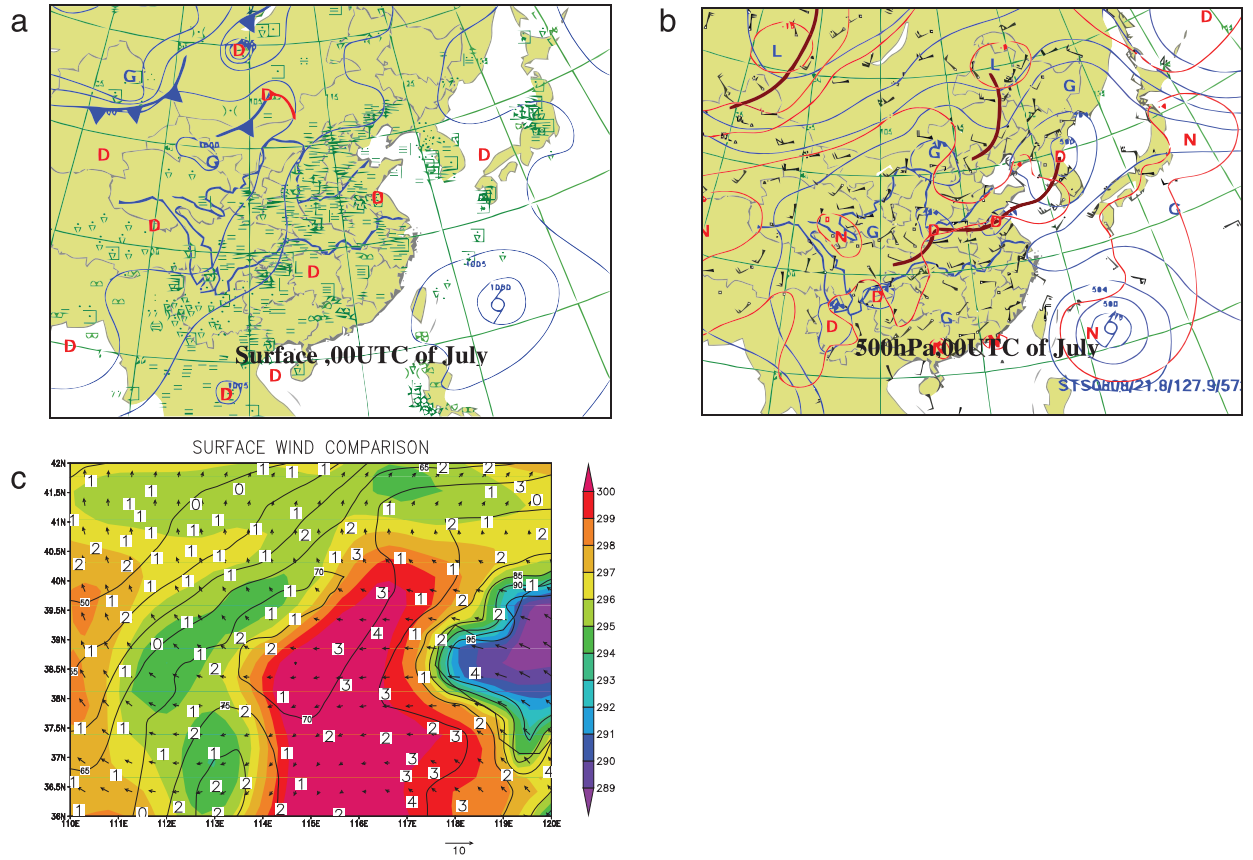

Fig. 4. (a) Typical weather charts at surface (left) and 500 hPa (right) (at 00UTC of July 26) in the hazy pollution episode. The subtropical high is marked by 588GPDM at 500 hPa and (b) the simulated mean wind (vector), temperature (shaded), humidity fields (contour) and observed wind speeds (scattered numbered) from July 22 to July 31.

north edge of the subtropical high marked by the line of 588 decametres of geopotential height (GPDM) (Fig. 4a, right) while the surface map indicated a weak continental high marked by the isobaric line of 1008 hPa (Fig. 4a, left). Fig. 4b shows the simulated mean wind, temperature, humidity fields and observed wind speeds from July 22 to July 31. The results indicate that warm and humid air from east and south was blown into North China and stopped by the Yan Mountains in the north and Taihang Mountains in the west with very low surface wind speeds, producing a condition similar to the weather map during this period of time. Under such conditions, the air mass was very stable and pollutants were easily accumulated. Consequently, persistently high PM10 concentrations were observed in *Shangdianzi*, reaching 150 μg m^{-3} and in *Nanjiao*, reaching 250 μg m^{-3} or more (Fig. 3). For all the five stations, the episode mean PM10 concentrations were all higher than those before the episode, i.e. the episode mean PM10 in *Shangdianzi* was more than four times higher than that before the episode.

Wind is the ultimate factor to determine the atmosphere stability and a control factor for pollutants' dispersion and diffusion. Figure 5 shows the time-height sectional wind field for Shangdianzi station before and during the heavy episode. Before the episode, a systematic high wind above brought an unstable condition into the region (Fig. 5a), favouring the diffusion and ventilation of the pollutants and resulting in a low PM concentration. However, during the episode, a reverse condition formed, featuring a low wind aloft and relatively large wind right above the surface (Fig. 5b). While the low wind aloft resulted in a systematic stable condition favourable for the accumulation of pollutants in the surface, the relatively high surface wind enhanced the mixing of pollutants in the boundary layer and transported the pollutants from urban source region to the rural stations. These contrast meteorological conditions were both observed and simulated for the Shangdianzi station and explained the reason for the formation of the episode and for the high rural PM concentrations observed.

Conversely, if the simulated conditions do not match the pollutant accumulation conditions, the model will under estimate the pollutant concentrations. This is clearly shown

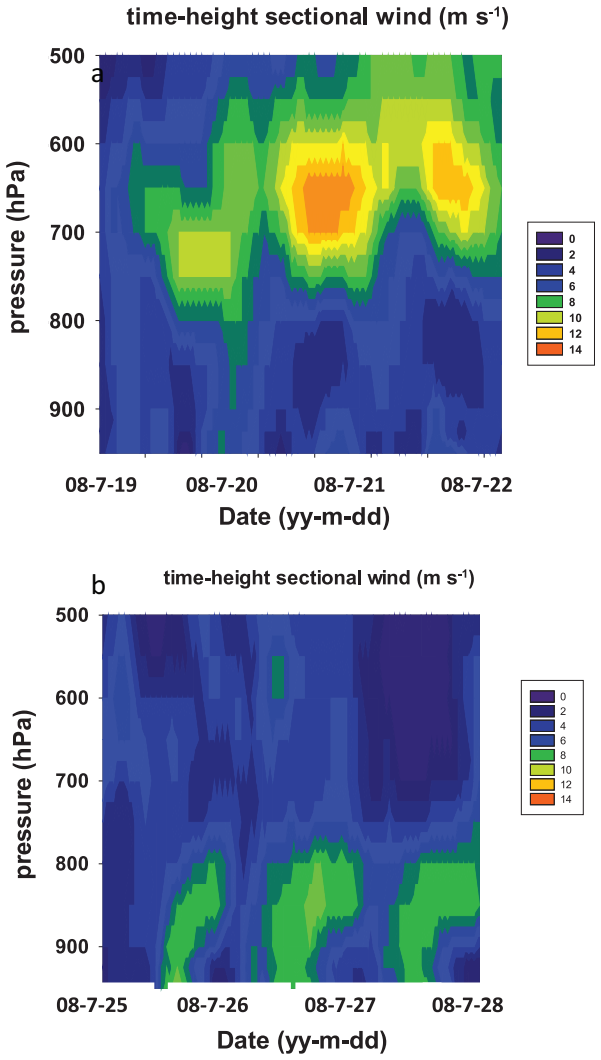

Fig. 5. The time-height sectional wind field for Shangdianzi. (a) Before the haze episode (July 19–22); (b) during the haze episode July 22–25; (c) during the haze episode (July 25–28).

for the CTL run which missed the episode. The time-height cross section wind indicated that a strong wind in the upper atmosphere was propagated downward gradually from July 23 to July 25, with a surface instant wind well above 14 m s^{-1} in Beijing and its neighbouring area on July 24 while the observed winds were only less than 4 m s^{-1} under 700 hPa at most time (Fig. 7a). In the surface there is a strong north wind belt invaded North China while most surface observations are about or less than 3 m s^{-1} (Fig. 7c). This false large wind field caused an abrupt drop in PM10 between July 24 and 25 in several stations, reaching below 50 μg m^{-3}, which was much smaller than the observed (Fig. 6). It also impacted on the pollution levels on July 25–28 because of the much lower pollutant initial conditions from the previous July 22–25 simulations.

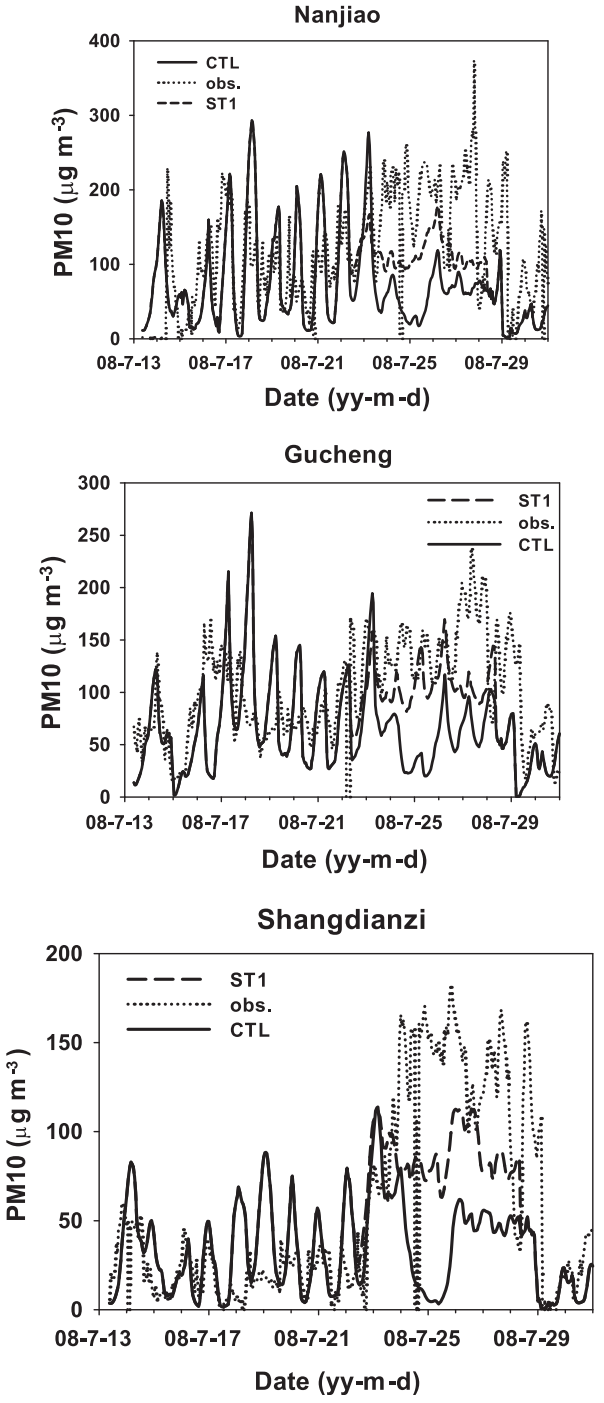

Fig. 6. Time series plot for simulated and observed hourly PM10 for Nanjiao(upper), Gucheng(middle panel) and Shangdianzi(bottom panel). Obs.(dotted) is the observed PM10, CTL(solid) is PM10 from the control run. ST1 (long dash) is PM10 from sensitive test one.

Although a low wind speed was simulated for July 25–28 in the low troposphere (Fig. 7b), the simulated PM10 was still much lower than the observed (Fig. 6).

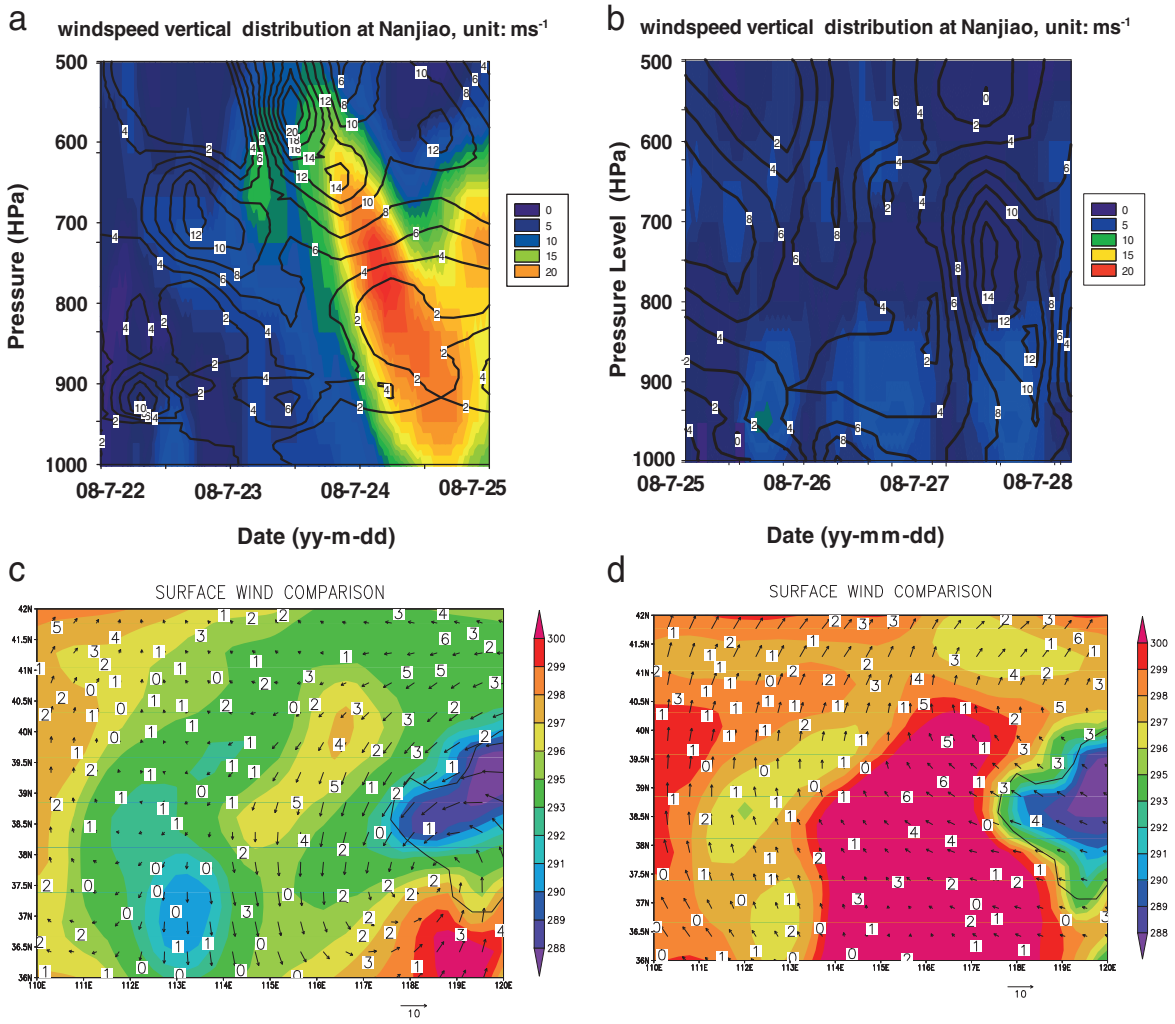

Fig. 7. The time-height sectional hourly wind speed (m s^{-1}) (shaded) and observed (contoured) from surface to 500 hPa for Nanjiao: (a) for 00Z July 22 to 00Z July 25 and (b) for 00Z July 25 to 00Z July 28. Simulated mean surface wind (vectored), temperature (shaded) and observed wind speed (scattered numbered) (c) for 08ZZ July 24 to 00Z July 25 and (d) for July 25 to 00Z July 28.

In order to improve the model results, the model was re-run (ST2) by replacing all the meteorology of July 22–25 with that of July 25–28, which was more close to the reality. The new results indicated that the correlation coefficients have obviously been increased from 0.4 to 0.84, −0.01 to 0.14, 0.2 to 0.54, 0.52 to 0.61 and 0.05 to 0.31 for *Shangdianzi, Nanjiao, Gucheng, Humin* and *Zhengzhou*, respectively, and a total correlation coefficient from 0.38 to 0.54 (Fig. 8). The time series of the PM10 concentrations are relatively persistently higher and much closer to the observation (Fig. 6).

It is further found that despite the use of more realistic meteorology, the underestimations still exist. This indicates that there is still much more space for the wind and the PBL conditions to be improved especially under the stable conditions.

3.5. *Evaluation of CUACE/Aero AOD*

3.5.1. Comparisons of AOD with remote sensing and surface-based measurements. In CUACE/Aero, the AOD was calculated from the simulated mass concentration, particulate size distribution, hygroscopic growth and absorbing and scattering properties of each size bin for every aerosol component. The output AOD is the sum of AOD of 12 bins of all aerosol species (i.e. dust, BC, OC, sea salt, sulphate, ammonium and nitrate) in the bands of 470, 550, 670, 870 and 1020 nm. Aerosol optical depth derived from

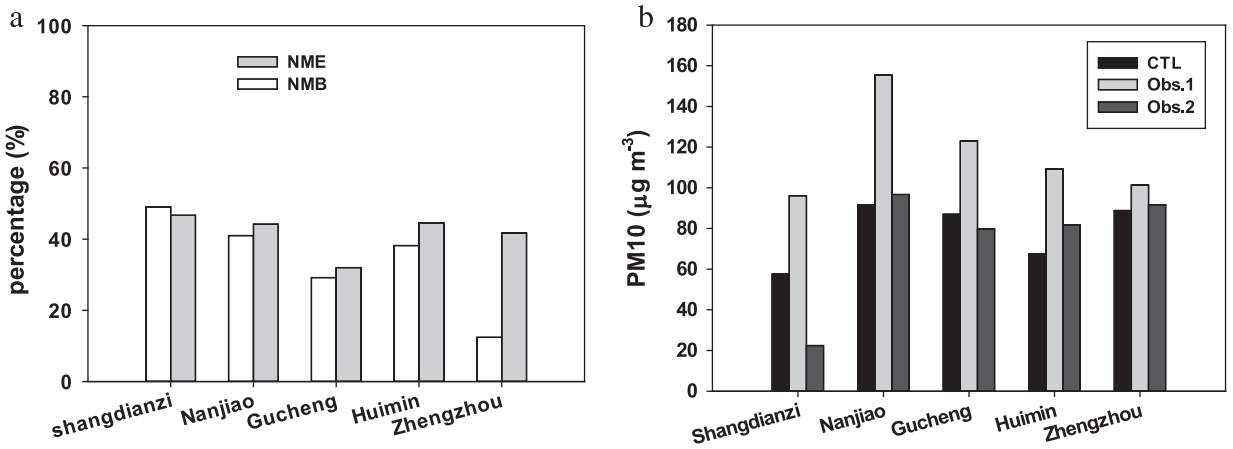

Fig. 8. (a) normalised mean bias (NMB) amplified –1 (white) and normalise mean error (NME)(grey) for each stations during the hazy polluted episode; (b) mean simulated PM10 (black) and mean observed PM10 (light grey) during the hazy polluted episode (July 22 to July 28) and mean observed PM10 (dark grey) before the episode (July 13 to July 21) for each stations in control run (CTL).

satellites is known for its higher spatial resolution and can represent the averaged aerosol distribution within a pixel and is often used to evaluate and to improve aerosol simulation (Jeuken et al., 2001; Kinne et al., 2003; Stier et al., 2005; Kinne et al., 2006). The level-2 AOD with a resolution of 10 km from MODIS (Kaufman, 1997a; Levy et al., 2007) satellite was used to evaluate CUACE AOD. Since NASA Terra overpasses China from 02:00 to 04:45 (UTC) each day, the mean CUACE AOD in three intervals, i.e. 02:00, 04:00 and 06:00, is selected for the comparisons when at least more than 15% MODIS AODs in 550 nm are available in a comparison model grid. Those AODs have been interpolated into the model grid by a search radius of 0.3°. Ground-based daily mean AODs in 440 nm at *Nanjiao*, *Shangdianzi*, *Gucheng*, *Huimin* and *Zhengzhou* stations (Che et al., 2009) from CARSNET are also used for the model AOD evaluations.

The correlation coefficient reaches 0.45 between modelled and MODIS AODs (Fig. 9a) and 0.23 between modelled and CARSNET AODs in CTL run (Fig. 9c). Statistically, the MBs and NMBs between model AOD and MODIS and CARSNET are all found to be positive with similar NMB and NME (Table 7, CTL), which indicates a systematic overestimation. The averaged CUACE AOD is about 116% higher than the MODIS and about 78% higher than the CARSNET. This was contrary to the averaged PM10 concentrations at daytime from the model, which were found to be underestimated with −39% of NMB and 45% of NME (Table 7, CTL). Although AOD represents the total column of the atmospheric aerosol loading, the highest loading is still concentrated near the surface layer, which makes a large contribution to AOD. Theoretically, a lower PM10 should result in a lower AOD.

Considering the strong capacity of fine particles, particularly those with diameter less than 1 μm, in absorbing and scattering sunlight and their great contributions to AOD, the error in the simulated number concentrations of fine particles would cause a large bias in AOD simulations. Monthly mean particle size distributions of water-soluble aerosols (<1 μm in diameter) of sulphate, nitrate, OC and ammonium from 5-minute intervals raw data measured in a field campaign carried out at the same period in Beijing by an AMS (Zhang et al., 2009) were used to compare the size distribution of water-soluble aerosols simulated by CUACE/Aero. The result showed that the peak of the simulated size distribution of fine particles was close to 0.1 μm which was coinciding with the size where the peak particle extinction coefficient was while the peak of the

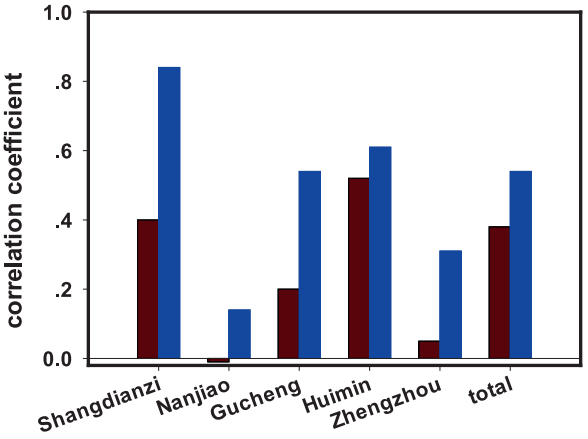

Fig. 9. Correlation coefficients (significance level = 0.0500) for Shangdianzi, Nanjiao, Gucheng, Huiming, Zhengzhou and total (including all data) for control run (CTL; brown columns) and ST1.

Table 7. Simulated daytime mean (model mean) and observed daytime mean (observed mean), and MB (mean bias), NMB (normalised mean bias), NME (normalised mean errors and correlation coefficient r between AOD of control run (CTL) and sensitive test two (ST2) with those of MODIS and CARSNET

Aerosol constituent	Model mean	Observed mean	MB	NMB (%)	NME (%)	r
MODIS						
CTL	1.40	0.65	0.75	116	143	0.45
ST2	0.81	0.65	0.16	25	76	0.44
CARSNET						
CTL	2.71	1.54	1.17	78	111	0.23
ST2	1.37	1.54	−0.17	−11	62	0.31
PM10						
CTL	56.3	92.2	−36.0	−39.0	45.0	0.52
ST2	55.2	92.2	−37.0	−37.1	46.1	0.49

Significance level = 0.0500.

observed particle size distribution was close to 0.5 μm, with much narrower spectral width (Fig. 10c). Though the simulated peak mass concentration was less than a half of the observed one, the simulated number concentration was still about two orders higher. With the same prescribed extinction parameters, the simulated extinction of water-soluble aerosols (<1 μm) should be much higher than the one if the observed size distribution was used, resulting in the over-estimation of predicted AODs. Therefore, the number size distribution is one of the most sensitive parameters for the overestimated AODs.

3.5.2. The effect of initial size distribution on AOD simulations. Mass size distributions for anthropogenic aerosols after emissions are usually prescribed from hypothesis or from observations near the source. Currently, most are based on the observation and laboratory work in Europe and North America where the annual mean concentration is typically about 20 μg m^{-3} (Malm et al., 2004; Torseth, 2004), much lower than those in east Asia where the annual mean for most stations can reach up to more than 100 μg m^{-3} (Qu et al., 2010). The initial mass size distribution in China may be quite different from those of Europe and North America. A new set of initial mass and number probability density function (PDF) of anthropogenic aerosols emitted was constructed (ST2) to explore the reasons of the overestimated AOD in CTL run.

In CTL, the prescribed mass size distribution for all the mass and AOD results discussed before is following the idealised log-normal mass size distributions:

$$f_x = \frac{1}{\sigma\sqrt{2\pi}} exp\left(-\frac{(\log 10(x)-\mu)^2}{2\sigma^2}\right),\ x>0$$

The mass mean diameter μ was 0.1 μm for BC and OC (Berner et al., 1996), 0.25 μm for sulphate and nitrate and 3 μm for fugitive dust (Fig. 11). The MSE for all these components was 1.7. In ST2, the mass size distributions were reconstructed from the integrated size distribution observations in the summer time from 2004 to 2006 from 3 nm to 10 μm during the CAREBeijing-2006 (Yue et al., 2009) and 2008 intensive observation at CMA as shown in Figure 12. Compared to the previous distributions, the peak size of the new mass size distribution for BC, OC, sulphate and nitrate is changed from 0.1 to 0.5 μm and the peak PDF values changed from $\sim$50 to 25%, displaying more evenly in the range of 0.01–0.1 μm.

In both the CTL and ST2 runs, the initial mass size distributions for natural dust and sea salt remain unchanged. The dust is set to be in three log normal distributions with the mean diameter of 1.99, 4.56 and 7.68 μm and the MSE of 0.96, 0.62 and 0.21, respectively from the detailed observations in Asia dust source area (Zhang et al., 1998). The emission size distribution for sea salt is computed through the density function of size and wind at 10 m high (Gong, 2003).

The re-run results (ST2) showed that the averaged PM10 was only reduced by 1.1 μg m^{-3} and the NMB difference was only 1%, indicating the negligible impact of the new size distribution on the total PM10 mass. However, the difference between AODs from the two size distributions was quite obvious (Table 7). The averaged AOD was reduced from 1.40 to 0.81 when compared with MODIS, which was much closer to the observed mean 0.61 than before. The MB was decreased to $\sim$1/5 of the original value and NMD by $\sim$50%. Compared with CARSNET, the averaged AOD reduced from 2.71 to 1.37, changing from 78% overestimation to 11% underestimation, with only half of the original NME. The over-estimation of AOD at daytime has been corrected. The correlation coefficient between modelled AOD and CARSNET AOD

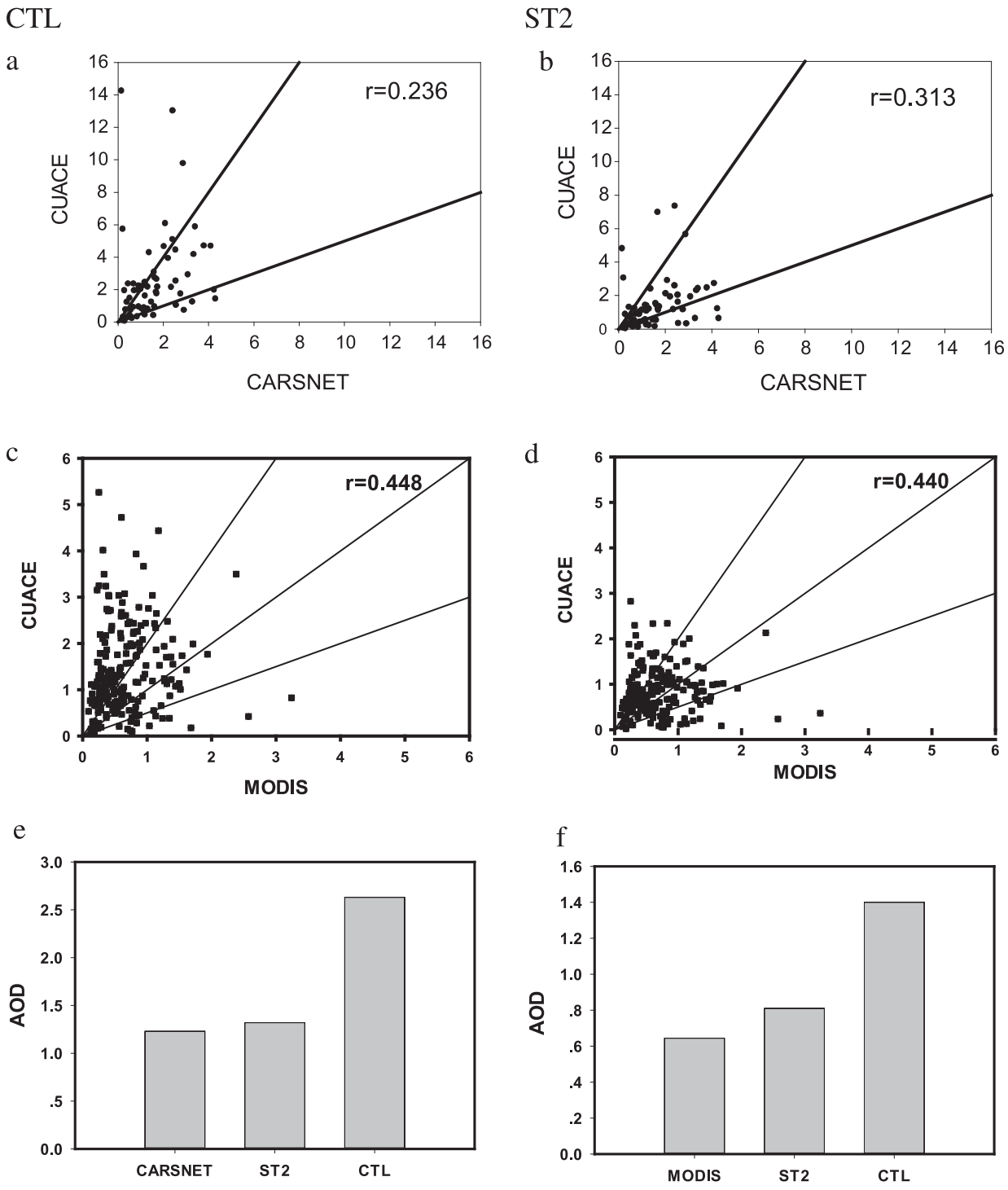

Fig. 10. (a, b, c and d): scattered plots between CUACE AOD and CAERSNET AOD, CUACE AOD and MODIS AOD; (e and f): vertical bar plots for mean values of CUACE AOD, CARSNET AOD and MODIS AOD. Results of CTL means from the control run and results of ST2 means with the new size distribution.

was increased from 0.23 to 0.31, with little change to the MODIS correlations. The scatter plots (Fig. 10b, d) show the obvious improvements of modelled AOD, especially with MODIS, and the original overestimated AODs are now evenly distributed within a factor of 2 from the observed. Therefore, the more realistic size distributions

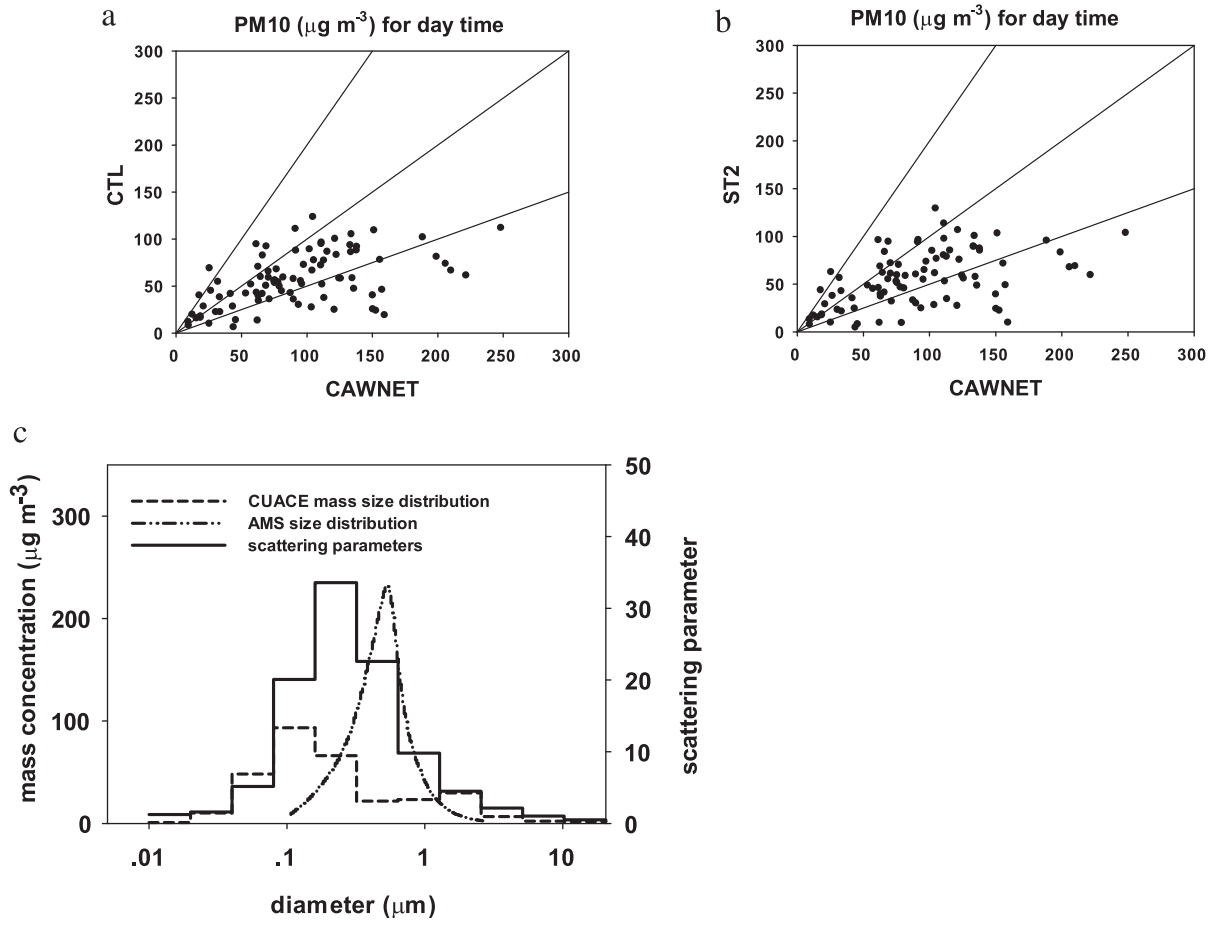

Fig. 11. Scattered plots for daytime mean PM10 between the simulated and observed of all the CAWNET five stations, (a) for the control test (CTL) and (b) for the sensitive test two (ST2) with the new size distribution; (c) for the observed mass size distribution, prescribed mass size distribution and aerosol scattering capacity.

greatly improve the AOD simulation without much influence on the total PM10 predictions.

It was also found the new initial size distribution did not bring the AOD calculation into the same systematic under-estimation as the total PM10. This may be related to the vertical profiles of the aerosols and the total aerosol column loading. One possibility was that the daytime aerosol loading may be overestimated, resulting in the higher AOD, even with underestimated PM10 in the surface. However, due to the lack of vertical profile observations, this cannot be verified at present. Therefore, in addition to having a more realistic aerosol size distribution, the observed vertical profiles are also very important in improving the AOD calculations, i.e. the CALIPSO may provide further information for the model impartment.

3.5.3. Size distribution on the contribution of each aerosol type to the total AOD. The modelling results enable the analysis of the contribution of each aerosol type to the total AOD. It is shown that sulphate is the dominant contributor to the total AOD in Beijing (Fig. 13), followed by OC, dust and BC. The contribution of sea salt can be ignored. The new initial size distribution reduced the AODs of BC, OC and dust by about 60% and of sulphate by 53%. One of the reasons for the difference may be due to the fact that most of the sulphate is from the oxidation of SO_2 and subsequent gas-to-particle conversion process such as nucleation, coagulation and condensation. The change in the size distribution of existing particles will change the condensation process of sulphuric acid and indirectly change the sulphate size distribution, resulting in the lower AOD. Generally, the total AOD reduction is about 51% with less MB.

4. Summary and conclusions

China Meteorological Administration Unified Atmospheric Chemistry Environment/Aerosols, CUACE/Aero,

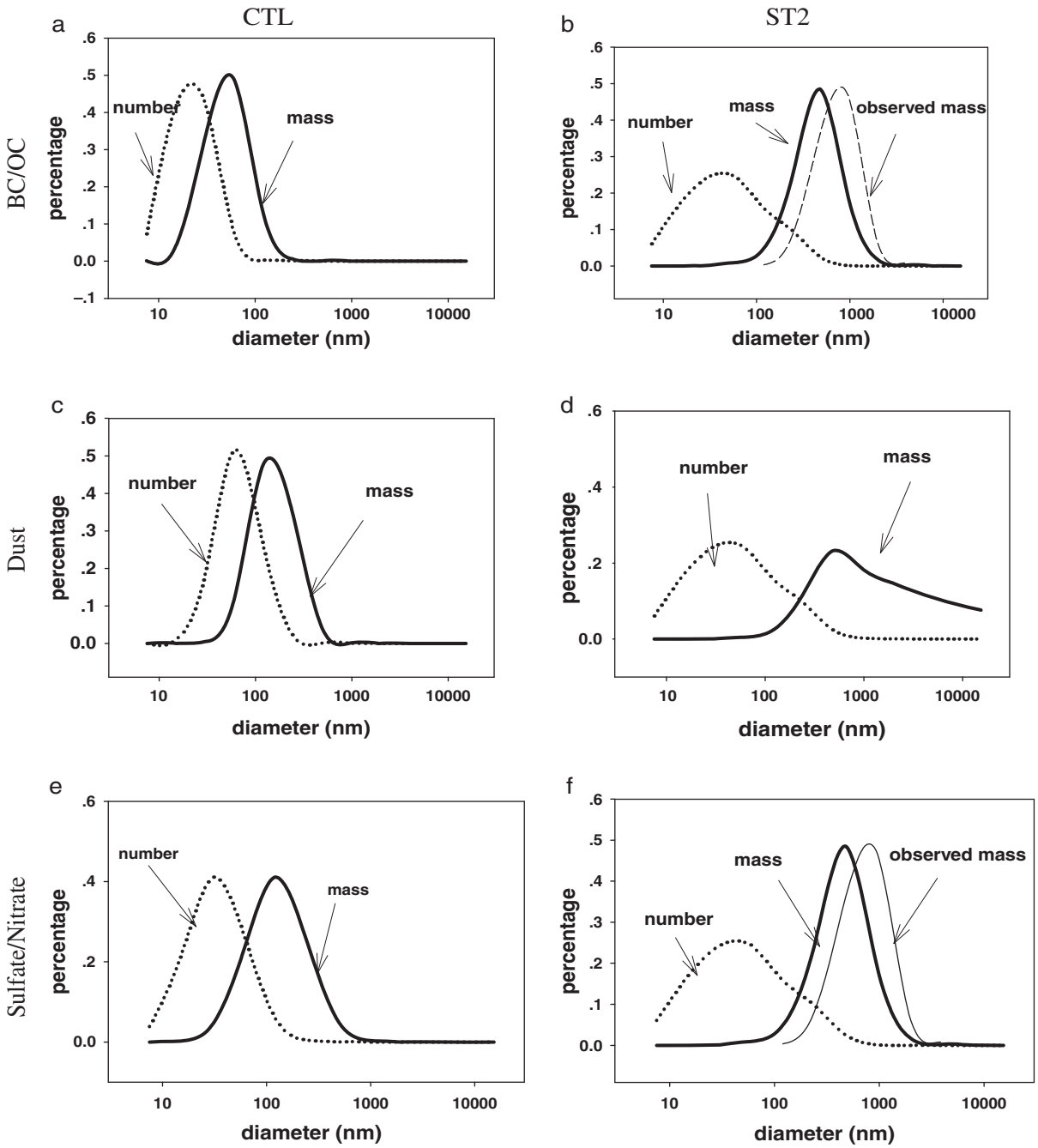

Fig. 12. The size and mass probability density function (PDF) distributions for BC and OC (a and b), fugitive dust (c and d), and sulphate and Nitrate (e and f). Observed mass are for the mean observed mass size distribution at the site of CMA during the test time.

has been developed with fully online coupled gas phase chemistry, aerosol microphysics and thermodynamic equilibrium. Applied in North China and evaluated with observational data, the factors influencing the performance of the model are investigated with improvements proposed to enhance the model ability to predict both aerosol chemical and optical properties.

It is found that the model captured the general variations of PM10 with most of the data within a factor of 2 from the observations and a combined correlation coefficient (r) of 0.38 when compared the hourly and daily averaged PM10 from five stations in North China. The correlation between simulated and observed PM10 is better at daytime than at nighttime and better at rural than at urban sites.

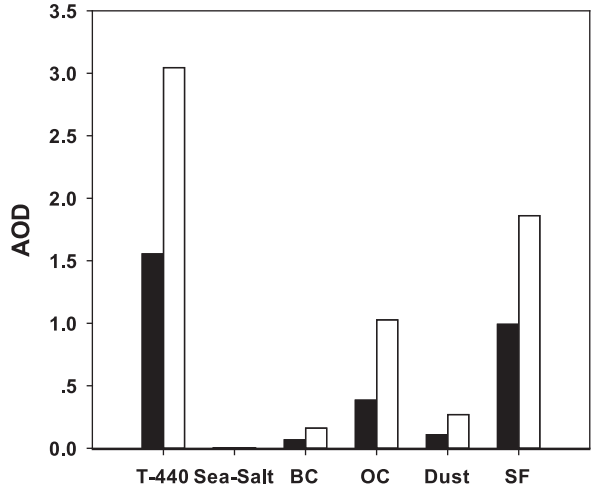

Fig. 13. Total AOD and AOD of Sea-Salt, BC, OC, Dust and SF at 440 nm wavelength for control test (CTL) (white) and sensitive test 2(ST2) (black).

Uncertainty in night emissions as well as model resolution to resolve the heterogeneous features in the urban areas are attributed for the difference. Another factor for the systematic underestimation of daytime PM10 concentrations is from the overestimation in simulating the PBL heights at daytime, i.e. over 1500 m versus observed 1000 m. At night, random errors dominated because PBL heights are always about 40 m with little variations in the meteorological model, neglecting the in-homogeneous factors such as the night turbulence and heat island impacts over a large area of the city.

The comparison of sub-micron aerosol compositions with AMS measurements in Beijing shows a systematic underestimation of sulphate, nitrate and ammonium concentrations by $\sim$60, 70 and 96%, respectively. This was primarily due to the weaker, simulated OH concentrations and less ammonia emission estimation in Beijing. OC simulation results are rather reasonable with only 10% bias while the BC concentration was about 129% higher than observed.

It is found that the accuracy of meteorological simulations is the key to capture the heavy pollution episodes. The PM10 concentrations during July 23–25 in the heavy pollution episode were severely underestimated due to an incorrect simulation of strong winds in the surface and aloft that caused the unrealistic dispersion and resulted in a quick drop in pollutant concentrations. Corrected with more realistic meteorology, this underestimation was greatly improved, although the uncertainties still existed. Further analysis of emission, transformation, deposition processes as well as sub-grid treatment is needed to narrow the difference for heavy pollution simulations.

On the basis of the observations of aerosol mass size distributions, a more realistic size distribution for the primary particle emissions of BC, OC, sulphate and nitrate aerosols was constructed. The new size distribution of primary emissions shifted the peak concentration from 0.1 to 0.5 μm and greatly improved the AOD simulations over the original results where an overestimation was found for all sites despite of the underestimation of the daytime PM10 mass concentrations. Though this study pointed out the direction towards improving the simulation of the aerosol size distributions and AOD, further study is still needed to obtain more information on the size distributions of primary particle from different regions and industrial sectors.

This work also reveals the comparability of simulated AOD with observations. The correlation coefficient between simulated AOD is 0.45 with MODIS but is only 0.23 with surface CARSNET AODs, indicating that the simulated AOD is more comparable with the grid-averaged AOD by MODIS (10 km grid average) than with the single-point measurement by CARSNET.

It should be pointed out that this paper only uses the surface data to evaluate the PM10 chemical compositions. The vertical profiles and column loading data should be used in the future to further the understanding of the model processes of AOD and aerosol–cloud interactions.

5. Acknowledgements

The authors wish to thank for the financial support from the National Basic Research Program (973) of China (2011CB403404), CAMS Basic Research Project (2010Z001, 2010Z002) for this work.

References

Adams, P. J., Seinfeld, J. H., Koch, D., Mickley, L. and Jacob, D. 2001. General circulation model assessment of direct radiative forcing by the sulfate-nitrate-ammonium-water inorganic aerosol system. *J. Geophys. Res.* **106**, 1097–1111.

Alfaro, S. C. and Gomes, L. 2001. Modeling mineral aerosol production by wind erosion: emission intensities and aerosol size distribution in source areas. *J. Geophys. Res.* **106**, 18075–18084.

Berner, A., Sidla, S., Galambos, Z., Kruisz, C., Hitzenberger, R. and co-authors. 1996. Modal character of atmospheric black carbon size distribution. *J. Geophys. Res.* **101**, 19559–19565.

Bertrand, C., Vanypersele, J. P. and Berger, A. 2002. Are natural climate forcings able to counteract the projected anthropogenic global warming? *Clim. Change* **55**, 413–427.

Brook, R. D., Brook, J. R., Urch, B., Vincent, R., Rajagopalan, S. and co-authors. 2002. Inhalation of fine particulate air pollution and ozone causes acute arterial vasoconstriction in healthy adults. *Circulation* **105**, 1534–1536.

Caminade, C., Terray, L. and Maisonnave, E. 2006. West African monsoon response to greenhouse gas and sulphate aerosol forcing under two emission scenarios. *Climate Dynamics* **26**, 531–547.

Cao, G. L., An, X., Zhou, C., Ren, Y. and Tu, J. 2010. Emission inventory of air pollution in China. *China Environ. Sci.* **30**(7), 900–906.

Cao, G. L., Zhang, X. Y., Wang, Y. Q., Che, H. Z. and Chen, D. 2005. Inventory of atmospheric pollutants discharged from biomass burning in China continent. *China Environ. Sci.* **24**, 389–393 (in Chinese).

Cao, G. L., Zhang, X. Y., Wang, Y. Q., Che, H. Z. and Chen, D. 2006. Inventory of black carbon emission from china. *Adv. Cli. Change Res.* **2**, 259–264 (in Chinese).

Carmichael, G. R., Sakurai, T., Streets, D., Hozumi, Y., Ueba, H. and co-authors. 2008. MICS-Asia II: the model intercomparison study for Asia Phase II methodology and overview of findings. *Atmos. Environ.* **42**, 3468–3490.

Charlson, R. J. and Heintzenberg, J. 1995. *Aerosol Forcing of Climate*. John Wiley & Sons, Berlin.

Che, H., Zhang, X., Chen, H., Damiri, B., Goloub, P. and co-authors. 2009. Instrument calibration and aerosol optical depth validation of the China Aerosol Remote Sensning Network. *J. Geophys. Res.* **114**, D03206, doi: 03210.01029/02008JD011030.

Chin, M., Ginoux, P., Lucchesi, R., Huebert, B., Weber, R. and co-authors. 2003. A global aerosol model forecast for the ACE-Asia field experiment. *J. Geophys. Res.* **108**(D23) 8654, doi: 8610.1029/2003JD003642.

Crawford, J., Olson, J., Davis, D., Chen, G., Barrick, J. and co-authors. 2003. Clouds and tracer gas distribution during TRACE-P. *J. Geophys. Res.* **108**, 8818, doi: 8810.1029/2002JD003177.

Cressman, G. P. 1959. An operational objective analysis system. *Mon. Weather Rev.* **97**, 367–374.

Dilley, G., Dennis, E., McNally, E. D., Tesche, T. W. and Morris, M. R. (2003). Air quality modeling analysis for the Denver early action ozone compact: Evaluation of MM5 simulations of the summer '02 Denver ozone season and embedded high 8-hr ozone episodes. *Environ. Alph. Geophys.*

Fast, J. D., Gustafson, W. I. G., Jr., Easter, R. C., Zaveri, R. A., Barnard, J. C. and co-authors. 2005. Evolution of ozone, particulates, and aerosol direct radiative forcing in the vicinity of Houston using a fully coupled meteorological-chemistry-aerosol model. *J. Geophys. Res.* **111**, D21305, doi: 21310.21029/22005JD006721.

Gery, M. W., Whitten, G. Z., Killus, J. P. and Dodge, M. C. 1989. A photochemical kinetics mechanism for urban and regional scale computer modeling. *J. Geophys. Res.* **94**(D10), 12925–12956.

Gong, S. L. 2003. A parameterization of sea-salt aerosol source function for sub- and super- micron particles. *Global Biogeochem. Cycles* **17**, 1097, doi: 1029/2003GB002079.

Gong, S. L., Barrie, L. A., Blanchet, J.-P., Salzen, K. v., Lohmann, U. and co-authors. 2003a. Canadian aerosol module: a size-segregated simulation of atmospheric aerosol processes for climate and air quality models 1. Module development. *J. Geophys. Res.* **108**, 4007, doi: 4010.1029/2001JD002002.

Gong, S. L., Zhang, X. Y., Zhao, T. L., McKendry, I. G., Jaffe, D. A. and co-authors. 2003b. Characterization of soil dust distributions in China and its transport during ACE-ASIA 2. Model Simulation and Validation. *J. Geophys. Res.* **108**, 4262, doi: 4210.1029/2002JD002633.

He, Q., Mao, J., Chen, J. and Han, S. 2006. A study of evolution and dynamics of urban atmospheric mixing-layer depth based on lidar data and numerical simulation. *Chinese J. Atmos. Sci. (In Chinese)* **22**, 293–306.

Hong, S.-Y. and Noh, Y. 2006. A new vertical diffusion package with an explicit treatment of entrainment progresses. *Mon. Weather Rev.* **134**, 2318–2341.

IPCC. 2007. Climate Change 2007: the physical science basis. In: *Contribution of Working Group I to the Fourth Assessment Report of the Intergovernmental Panel on Climate Change*. Cambridge University Press, Cambridge, UK and New York, NY, USA, 996 pp.

Jacobson, M. Z. 1997. Development and application of a new air pollution modeling system. Part III: aerosol-phase simulations. *Atmos, Environ.* **31**(4), 587–608.

Jeuken, A., Veefkind, J. P., Dentener, F., Metzger, S. and Gonzalez, C. R. 2001. Simulation of the aerosol optical depth over Europe for August 1997 and a comparison with observations. *J. Geophys, Res.* **106**(D22), 28295–28311.

Jones, A., Roberts, D. L. and Slingo, J. 1994. A climate model study of indirect radiative forcing by anthropogenic sulphate aerosols. *Nature* **370**, 450–453.

Kaufman, Y. J., Tanre, D., Vermote, L. A., Chu, A. and co-authors. 1997a. Operational remote sensing of tropospheric aerosol over land from EOS moderate resolution imaging spectroradiometer. *J. Geophys. Res.* **102**(D14), 17051–17067.

Khain, A. P. 2009. Notes on state-of-art investigations of aerosol effects on precipitation: a critical review. *Environ. Res. Lett.* **4**, 1–20, doi: 10.1088/1748-9326/1084/1081/015004.

Kinne, S., Lohnmann, U., Feichter, J., Schulz, M., Timmreck, C. and co-authors. 2003. Monthly averages of aerosol properties: a global comparison among models satellite data, and AERONET ground data. *J. Geophys. Res.* **108**(D20), 4634, doi: 4610.1029/2001JD001253.

Kinne, S., Schulz, M., Textor, C., Guibert, S., Balkanski, Y. and co-authors. 2006. An AeroCom initial assessment – optical properties in aerosol component modules of global models. *Atmos. Chem. Phys.* **6**, 1815–1834.

Lang, X.-L., Cao, G.-l. and Huang, X.-m. 2008. Inventory of NOX emissions from China. *Environ. Sustain. Dev.* **6**, 19–21 (in Chinese).

Levin, Z. and Cotton, W. R. 2009. *Aerosol Pollution Impact on Precipitation, a Scientific Review*. Springer, New York.

Levy, R. C., Remer, L. A., Mattoo, S., Vermote, E. F. and Kaufman, Y. J. 2007. Second-generation operational algorithm: retrieval of aerosol properties over land from inversion of Moderate Resolution Imaging Spectroradiometer spectral reflectance. *J. Geophys. Res.* **112**, D13211, doi: 13210.11029/12006JD007811.

Mahrt, L., Richardson, S., Seaman, N. and Stauffer, D. 2012. Turbulence in the nocturnal boundary layer with light and variable winds. *Q. J. R. Meteorol. Soc*. doi: 10.1002/qi.1884, (in press).

Malm, W. C., Schichtel, B. A., Pichford, M. L., Ashbaugh, L. L. and Eldred, R. A. 2004. Spatial and monthly trends in fine particles concentration in the United States. *J. Geophys. Res*. **109**, D03306, doi: 03310.01029/02003JD003739.

Marticorena, B. and Bergametti, G. 1995. Modeling the atmospheric dust cycle. Part 1: Design of a soil-derived dust emission scheme. *J. Geophys. Res*. **100**, 16415–16430.

Nakajima, T., Yoon, S.-C. and Ramanathan, V. 2007. Overview of the atmospheric Brown Cloud East Asian regional experiment 2005 and a study of the aerosol direct radiative forcing in East Asia. *J. Geophys. Res*. **112**, D24S91, doi: 110.1029/2007JD009009.

Nenes, A., Pilinis, C. and Pandis, S. 1998. Continued development and testing of a new thermodynamics aerosol module for urban and regional air quality models. *Atmos. Environ*. **33**, 1553–1560.

Qu, W. J., Arimoto, R., Zhang, X. Y., Zhao, C. H., Wang, Y. Q. and co-authors. 2010. Spatial distribution and interannual variation of surface PM10 concentration over eight-six Chinese cities. *Atmos. Chem. Phys*. **10**, 5641–5662, doi: 5610.5194/acp-105641-102010.

Ramanathan, V., Crutzen, P., Kieh, J. and Rosenfeld, D. 2001. Aerosols, climate, and the hydrological cycle. *Science* **294**(5549), 2119–2124.

Ren, X., Wang, H., Shao, K., Miao, G. and Tang, X. 2002. Determination and characteristics of OH radical in urban atmosphere in Beijing. *Environ. Sci*. **23**, 24–27.

Richter, A., Burrows, J. P., Nüß, H., Granier, C. and Niemeier, U. 2005. Increase in tropospheric nitrogen dioxide over China observed from space. *Nature* **437**, 129–132, doi: 10.1038/nature04092.

Schell, B., Ackermann, I. J., Hass, H., Binkowski, F. S. and Ebel, A. 2001. Modeling the formation of secondary organic aerosol within a comprehensive air quality model system. *J. Geophys. Res*. **106**, 28275–28293.

Smolarkiewicz, P. K. 2006. Multidimensional positive definite advection transport algorithm: an overview. *Int. J. Numer. Method Fliud* **50**, 1123–1144.

Steeneveld, G. J., Hartogensis, O. K., Moene, A. F., Baltink, H. K. and Holtslag, A. A. M. 2008. Evaluation of WRF model improvements with novel boundary-layer observations – focus on diurnal cycle and stable boundary layer. *WRF Visitors Program Report*.

Stier, P., Feichter, J., Kinne, S., Kloster, S., Vignati, E. and co-authors. 2005. The aerosol-climate model ECHAM5-HAM. *Atmos. Chem. Phys*. **5**, 1125–1156.

Stockwell, W. R., Middleton, P., Change, J. S. and Tang, X. 1990. The second generation regional acid deposition model chemical mechanism for regional air quality modeling. *J. Geophys. Res*. **95**, 16343–16376.

Streets, D. G., Bond, T. C., Carmichael, G. R., Fernandes, S. D., Fu, Q. and co-authors. 2003. An inventory of gaseous and primary aerosol emissions in Asia in the year 2000. *J. Geophys. Res*. **108**, 8809, doi: 8810.1029/2002JD003093.

Tang, Y., Carmichael, G. R., Seinfeld, J. H., Dabdub, D., Weber, R. J. and co-authors. 2004. Three-dimensional simulation of inorganic aerosol distributions in east Asia during spring 2001. *J. Geophys. Res*. **109**, D19S23, doi: 10.1029/2003JD004201.

Torseth, K. 2004. *Transboundary Particulate Matter in Europe*. Status Report 4/2004, EMEP Report.

Tsai, F., Liu, T.-H., Liu, S. C., Chen, T.-Y., Anderson, T. L. and co-authors. 2004. Model simulation and analysis of coarse and fine particle distributions during ACE-Asia. *J. Geophys. Res*. **109**, D19S20, doi: 10.1029/2003JD003665.

Twomey, S. J. 1991. Aerosols, clouds and radiations. *Atmos. Environ*. **25A**, 2435–2442.

West, J. J., Pilinis, C., Nenes, A. and Pandis, S. N. 1998. Marginal direct climate forcing by atmospheric aerosols. *Atmos. Environ*. **32**, 2531–2542.

Wilcox, E., Roberts, G. and Ramanathan, V. 2006. Influence of Aerosols on the shortwave cloud radiative forcing from North Pacific oceanic clouds: results from the Cloud Indirect Forcing Experiment (CIFEX). *Geophys. Res. Lett*, **33**, L21804, doi: 10.1029/2006GL027150.

Yu, S. 2000. The role of organic acids (formic, acetic, pyruvic and oxalic) in the formation of cloud condensation nuclei (CCN): a review. *Atmos. Res*. **53**, 185–217.

Yu, S., Dennis, R., Nenes, S. R. A., Walker, J., Eder, B. and co-authors. 2005. An assessment of the ability of 3-D air quality models with current thermodynamic equilibrium models to predict aerosol NO3. *J. Geophys. Res*. **110**, D07S13, doi: 10.1029/2004JD004718.

Yu, S., Eder, B., Dennis, R., Chu, S. and Schwarts, S. 2006. New unbiased symmetric metrics for evaluation of air quality models. *Atmos. Sci. Lett*. **7**, 26–34.

Yu, S., Mathur, R., Schere, K., Kang, D., Pleim, J. and co-authors. 2008. Evaluation of real-time PM2.5 forecasts and process analysis for PM2.5 formation over the eastern United States Using the Eta-CMAQ forecast model during the 2004 ICARTT study. *J. Geophys. Res*. **113**, D06204, doi: 06210.01029/02007JD009226.

Yu, S., Saxena, V. K. and Zhao, Z. 2001. A comparison of signals of regional aerosol-induced forcing in eastern China and the southeast United States. *Geophys. Res. Lett*. **28**, 713–716.

Yue, D., Hu, M., Wu, Z., Wang, Z., Guo, S. and co-authors. 2009. Characteristic of aerosol size distribution ad new particle formation in the summer in Beijing. *J. Geophys. Res*. **114**, doi: 10.1029/2008JD010894.

Zhang, X. Y., Arimoto, R., Zhu, G. H., Chen, T. and Zhang, G. Y. 1998. Concentration, size-distribution and deposition of mineral aerosol over Chinese desert regions. *Tellus* **50B**, 317–330.

Zhang, Y., Seigneur, C., Seinfeld, H. H., Jacobson, M. Z. and Binkowski, F. S. 1999. Simulation of aerosol dynamics: a comparative review of algorithms used in air quality models. *Aerosol Sci. Technol*. **31**, 487–514.

Zhang, M., Umo, I., Carmichael, G. R. e. a. 2003. Large-scale structure of trace gas and aerosol distributions over the western Pacific Ocean during the Transport and Chemical Evolution

Over the Pacific (TRACE-P) experiment. *J. Geophys. Res.* **108**(D21), 8820, doi: 8810.1029/2002JD002946.

Zhang, X. Y., Wang, Y. Q., Niu, T., Zhang, X. C. and Gong, S. L. 2011. Atmospheric aerosols in China: spatial/temporal variability, chemical signature, regional haze distribution and comparisons with global aerosols. *Atmos. Chem. Phys. Discuss.* **11**, 26571–26615, doi: 26510.25194/acpd-26511-26571-22011.

Zhang, X. Y., Wang, Y. Q., Lin, W. L., Zhang, X. C., Gong, S. and co-authors. 2009. Changes of atmospheric composition and optical properties over Beijing. *Bull. Am. Meteorol. Soc.* **90**(11), 1633–1651.

Zhang, X. Y., Yang, Y. Q., Zhang, X. C., Guo, W. and Gong, S. L. 2008. Carbonaceous aerosol composition over various regions of China during 2006. *J. Geophys. Res.* **113**, D14111, doi: 14110.11029/12007JD009525.

Zhao, T. L., Gong, S. L., Zhang, X. Y. and McKendry, I. G. 2003. Modelled size-segregated wet and dry deposition budgets of soil dust aerosol during ACE-Asia, 2001: implications for Trans-Pacific Transport. *J. Geophys. Res.* **108**, 8665, doi: 8610.1029/2002JD003363.

Zhou, C. H., Gong, S. L., Zhang, X. Y., Wang, Y.Q., Niu, T. and co-authors. 2008. Development and evaluation of an operational SDS forecasting system for East Asia: CUACE/Dust. *Atmos. Chem. Phys.* **8**, 787–798.